Boundary-Layer Meteorol (2015) 157:219–236
DOI 10.1007/s10546-015-0063-3

ARTICLE

# Wind-Tunnel Study of Scalar Transfer Phenomena for Surfaces of Block Arrays and Smooth Walls with Dry Patches

**Juyeon Chung[1] · Aya Hagishima[1] · Naoki Ikegaya[1] · Jun Tanimoto[1]**

Received: 14 July 2014 / Accepted: 30 June 2015 / Published online: 14 July 2015


**Abstract** We report the result of a wind-tunnel experiment to measure the scalar transfer efficiency of three types of surfaces, wet street surfaces of cube arrays, wet smooth surfaces with dry patches, and fully wet smooth surfaces, to examine the effects of roughness topography and scalar source allocation. Scalar transfer coefficients defined by the source area $C_{\mathrm{E\,wet}}$ for an underlying wet street surface of dry block arrays show a convex trend against the block density $\lambda_{\mathrm{p}}$. Comparison with past data, and results for wet smooth surfaces including dry patches, reveal that the positive peak of $C_{\mathrm{E\,wet}}$ with increasing $\lambda_{\mathrm{p}}$ is caused by reduced horizontal advection due to block roughness and enhanced evaporation due to a heterogeneous scalar source distribution. In contrast, scalar transfer coefficients defined by a lot-area including wet and dry areas $C_{\mathrm{E\,lot}}$ for smooth surfaces with dry patches indicate enhanced evaporation compared to the fully wet smooth surface (the oasis effect) for all three conditions of dry plan-area ratio up to 31 %. Relationships between the local Sherwood and Reynolds numbers derived from experimental data suggest that attenuation of $C_{\mathrm{E\,wet}}$ for a wet street of cube arrays against streamwise distance is weaker than for a wet smooth surface because of canopy flow around the blocks. Relevant parameters of ratio of roughness length for momentum to scalar $B^{-1}$ were calculated from observational data. The result implies that $B^{-1}$ possibly increases with block roughness, and decreases with the partitioning of the scalar boundary layer because of dry patches.

**Keywords** Heterogeneity of source · Scalar Source · Scalar transfer coefficient · Wind-tunnel experiment

✉ Aya Hagishima
aya@cm.kyushu-u.ac.jp; ayahagishima@kyudai.jp

[1] Interdisciplinary Graduate School of Engineering Sciences, Kyushu University, 6-1, Kasuga-koen, Kasuga-shi, Fukuoka 816-8580, Japan

## 1 Introduction

Surface fluxes of momentum, heat, and other scalar quantities at urban rough surfaces are essential forcings of the urban atmospheric environment characterized by velocity, temperature, and scalar concentrations. Therefore, research involving an accurate estimation of such fluxes according to urban topography has been widely conducted for decades. Based on the similarity theory, the velocity profile over a fully rough surface under neutral stability is expressed by (e.g. Garratt 1994),

$$\frac{u}{u_*} = \frac{1}{\kappa} \ln\left(z/z_\mathrm{o}\right), \tag{1}$$

where $z_\mathrm{o}$ is the aerodynamic roughness length (m), $\kappa$ is the von Karman constant, and $u$ is wind speed (m $\mathrm{s}^{-1}$) at height $z$. The friction velocity $u_*$ is defined as $\sqrt{\tau_0/\rho}$, where $\tau_0$ and $\rho$ are surface shear stress (Pa) and the density of a fluid (kg $\mathrm{m}^{-3}$), respectively. The surface shear stress is sometimes expressed by the drag coefficient $C_\mathrm{m}$ as follows,

$$\tau_0/\rho = C_\mathrm{m}\, u^2. \tag{2}$$

As many previous studies have revealed, the geometry of urban roughness plays a significant role in the mean flow structure around urban obstacles, and the momentum absorption due to rough surfaces is mainly caused by the pressure drag, whilst the frictional drag is almost negligible. Therefore, the aerodynamic parameters $z_\mathrm{o}$ and $C_\mathrm{m}$ for urban surfaces are primarily determined by the geometry of the surface roughness as shown in past experimental work (e.g. Grimmond and Oke 1999; Cheng and Castro 2002; Hagishima et al. 2009; Zaki et al. 2011). Furthermore, both theoretical and empirical methodologies for predicting the urban roughness parameters based on several geometric parameters have been proposed (e.g. Macdonald et al. 1998; Millward-Hopkins et al. 2011; Kanda et al. 2013).

On the other hand, scalar transport processes, for example, vapour transport due to surface evaporation, can be expressed in a manner similar to Eq. 1 as follows.

$$\frac{q_\mathrm{surf} - q}{q_*} = \frac{1}{\kappa} \ln\left(z/z_\mathrm{os}\right), \tag{3}$$

where $q_\mathrm{surf}$ and $q$ are the specific humidity of the surface and air (kg $\mathrm{kg}^{-1}$), $z_\mathrm{os}$ is the scalar roughness length (m), $q_* = E/\rho u_*$, $E$ is the evaporation flux (kg $\mathrm{m}^{-2}\mathrm{s}^{-1}$). The ratio of $z_\mathrm{o}$ to the roughness length for the scalar is often expressed using the parameter $B$ as follows,

$$\kappa\, B^{-1} = \ln\left(z_\mathrm{o}/z_\mathrm{os}\right). \tag{4}$$

Alternatively, the scalar flux can be expressed using parameters related to the scalar transfer efficiency, such as the interfacial Dalton number $Da_0$, scalar transfer coefficient $C_\mathrm{E}$, and mass transfer coefficient $k$ (kg $\mathrm{m}^{-2}\mathrm{s}^{-1}$], as follows,

$$E = \rho\, Da_0 u_* \left(q_\mathrm{surf} - q\right). \tag{5}$$

$$E = \rho\, C_\mathrm{E} u \left(q_\mathrm{surf} - q\right). \tag{6}$$

$$E = k \left(q_\mathrm{surf} - q\right). \tag{7}$$

Note that the specific humidity $q$ included in Eq. 5 is originally defined at the upper boundary of the interfacial sublayer (e.g. Brutsaert 1975), where logarithmic profiles are applicable. Variables $u$ and $q$ included in Eq. 6 are principally determined by values within the inertial sublayer if $C_\mathrm{E}$ are used in the framework for the bulk transfer relations of the similarity theory, and in such cases, $C_\mathrm{E}$ is called the bulk transfer coefficient. Alternatively, $u$ and $q$ are

defined by values at an arbitrary height according to experimental conditions. Equation 7 is a widely used form in the mechanical engineering field, and $q$ is usually determined by the value of a reference location with little influence of the surface evaporation, such as above the boundary layer. The evaporation $E$ in Eqs. 5 and 6 mainly refers to the value per lot-area, while it is sometimes used as the value for a local point or a value per unit source area. Here, $Da_0$, $C_\mathrm{E}$, and $k$ are replaced by the interfacial Stanton number $St_0$, heat transfer coefficient $C_\mathrm{h}$, and convective heat transfer coefficient $h$ (W m$^{-2}$K$^{-1}$), respectively, for heat flux.

Unlike the momentum transport, scalar transport to and from rough surfaces is governed by molecular diffusion in the immediate vicinity of surfaces (e.g. Brutsaert 1982), thus, the Reynolds number dependency remains, albeit under the high Reynolds number condition. For example, Owen and Thomson (1963) investigated the relationship between the interfacial Stanton number and roughness Reynolds number $Re^*$, where $Re^* = u_* z_\mathrm{o}/\nu$, and $\nu$ is the kinetic viscosity, and presented a relation for $B^{-1}$ as an exponential function of $Re^*$. Chamberlain (1968) conducted a wind-tunnel experiment of deposition and evaporation on smooth and rough surfaces with various geometric conditions, and confirmed that the experimental results agree well with the relation presented by Owen and Thomson (1963). Brutsaert (1975) also derived a similar relationship between $B^{-1}$ and $Re^*$ from dimension analysis. Garratt and Hicks (1973) presented the relationship between $B^{-1}$ and $Re^*$ obtained by both wind-tunnel experiments on urban-like solid roughnesses and field measurements on permeable vegetation canopies, and pointed out the contrasting tendencies, where the data for solid roughnesses show an exponential relation, whilst vegetation canopies show a weaker dependency on $Re^*$.

More recently, Kanda et al. (2007) obtained information on $\kappa\, B^{-1}$ under the condition of high $Re^* \sim 10^5$ based on an outdoor experiment of block arrays with linear scales of 0.15 m and 1.5 m, much larger than those of previous wind-tunnel studies. They also proposed a new fitting curve between $\kappa\, B^{-1}$ and $Re^*$ for an urban setting with no vegetation. Additionally, Kanda and Moriizumi (2009) performed an outdoor experiment using block arrays with various geometries, and estimated $\kappa\, B^{-1}$, as well as the transfer coefficients for momentum $C_\mathrm{m}$ and heat $C_\mathrm{h}$. They pointed out that $C_\mathrm{h}$ is less sensitive to the change of geometry compared to $C_\mathrm{m}$, and the estimation of $C_\mathrm{h}$ derived from both the $z_\mathrm{o}$ calculated as a function of geometric parameters (Macdonald et al. 1998), and the $\kappa\, B^{-1} - Re^*$ relationship provides relatively good accuracy.

While numerous studies imply that the scalar transfer coefficients of urban-like rough surfaces can be primarily estimated through $Re^*$, the geometric dependency of the scalar transport parameters such as $\kappa\, B^{-1}$ and $C_\mathrm{E}$ is still in question. For instance, Anderson (2013) reviewed previous experimental data of scalar transport on rough surfaces, and pointed out that the scalar transfer efficiency varies with surface topography in spite of similar $Re^*$ conditions. Furthermore, because of recent developments in the urban canopy parametrization for mesoscale modelling, as well as the increase in computational fluid dynamics (CFD) simulations that explicitly resolve urban obstacles, accurate estimation of the transport efficiency of each surface of urban roughness, such as streets, building walls, and roofs, has become the primary focus of many studies.

For instance, Barlow and Belcher (2002) introduced a naphthalene sublimation technique to investigate the scalar transfer from an isolated two-dimensional (2D) street cavity sited perpendicular to the mean flow in a wind-tunnel. They revealed that the transfer speed is affected by the street-aspect ratio, and showed the effectiveness of this type of experiment to directly quantify the area-averaged scalar fluxes. Similarly, Barlow et al. (2004) measured the transfer coefficients of a street, walls, and a roof of 2D canopies consisting of multiple rods using the naphthalene sublimation technique. Their results were shown in terms of the effect

of street-aspect ratio on the transfer speed. In addition, the effect of scalar source allocation at the surface surrounding the measurement target on the scalar flux was investigated. Pascheke et al. (2008) made measurements of scalar concentration over block arrays, where the scalar is emitted from a naphthalene-coated surface on street surfaces, and they pointed out the significant effect of the height variability on dispersion. Narita (2007) introduced the water evaporation method to the measurement of evaporation rate from surfaces of both 2D and 3D block arrays. He investigated various effects of surface scalar transfer, such as street-aspect ratio, distance from the upwind edge of block arrays, position of canopy surfaces (roof, windward wall, leeward wall, and side wall), and wind direction. Hagishima et al. (2005) performed comparisons of past observations of transfer coefficients for surfaces of both scaled models in wind-tunnels and real buildings, and pointed out that the relationship between the street-aspect ratio and mass transfer coefficients of walls of 2D block arrays given by several previous wind-tunnel studies using different methods are close to consistent with one another. In addition, they suggested that the scalar source allocation on the canopy surface has a significant influence on the spatial distribution of the mass transfer coefficients for surfaces made up of a 2D canopy based on the comparison between two previous experiments. Ikegaya et al. (2012) conducted an experiment of the scalar transfer coefficients of street surfaces of several types of block arrays using the salinity method. They examined the effect of the layout of 3D block arrays, the height variability, and the randomness of rotation angles of blocks on scalar transfer coefficients.

In addition to these wind-tunnel experiments, CFD techniques have been recently utilized to investigate the transport phenomena of not only momentum but also heat and other scalar quantities around a building and urban-like block arrays. Blocken et al. (2009) and Defraeye et al. (2010, 2011) applied the Reynolds-averaged Navier–Stokes (RANS) equations coupled with a low Reynolds number turbulence model to investigate the spatial distribution of the convective heat transfer coefficient around an isolated building located on a flat plane. Pillai and Yoshie (2012) performed simulations of forced convection over regular block arrays using the RANS model coupled with a low Reynolds number turbulence model, and estimated the convective heat flux of each surface of the block arrays, including roofs, walls, and streets, with different block density conditions at various streamwise positions, after validation based on data from their wind-tunnel experiment.

In the context of recent research developments mentioned above, our study intends to answer the question of how the density of urban roughness affects the scalar transfer efficiency of a street surface, which arises from the inconsistency of the past three studies. The details and relevant studies are described in Sect. 2, and the measurement conditions and procedures are outlined in Sect. 3. The results and a discussion of the effects of roughness density and scalar source partitioning on the scalar transfer coefficients are presented in Sect. 4. Brief conclusions are given in Sect. 5.

## 2 Objectives

We focus on the following three studies in terms of the relationship between scalar transfer efficiency of streets of block canopies and the roughness density. The first is that of Barlow et al. (2004), which shows the transfer coefficients for facets of 2D block arrays with four conditions of street aspect ratios, $H/W = 0.25$, 0.5, 1 and 2 based on the naphthalene sublimation technique. Their results indicate that the transfer efficiency of street surfaces monotonically decreases as the canopy deepens, if an upstream wall adjacent to the target

street surface is also the source of the naphthalene emission. In contrast, for the case of a single street source, namely that the street surface for the measurement target is the only source of the scalar emission, the transfer efficiency shows a positive peak against the street-aspect ratio at $H/W = 1$. The second experimental result is based on a salinity evaporation experiment of Ikegaya et al. (2012), where a saline water surface is used as the scalar source, and the surfaces of block walls and roofs are completely dry. Their results indicate that $C_E$ for a street surface of cubical staggered arrays shows a positive peak against the plan-area density (ratio of roof area to total lot-area, hereafter $\lambda_p$) at $\lambda_p = 17$ %, similar to Barlow et al. (2004), and the measured values of $C_E$ for street surfaces of all block arrays are larger than for a smooth wet surface. They pointed out that their result might be attributed to two contrasting effects of urban roughness on scalar transfer: (1) a reduction of horizontal advection due to momentum absorption, leading to a decrease in $C_E$, and (2) turbulent mixing, which increases $C_E$. On the other hand, the numerical study of Pillai and Yoshie (2012) suggests a different tendency. The convective heat flux of each surface of a 3D block array derived from the RANS simulation decreases monotonically against $\lambda_p$ for 6, 11, 25, and 44 %. The wall boundary conditions in their simulation are determined based on their wind-tunnel experiment where blocks and street surfaces are heated, thus surfaces of streets as well as blocks are assumed to be the heat sources.

The main objective herein is to address the question of how the density of urban roughness acts on the scalar transfer efficiency of street surfaces. We designed the experimental plan based on the hypothesis that the difference in the location of the scalar source in each experiment is a cause of the discrepancy. The measurement devices and procedures in a wind-tunnel experiment similar to those used in Ikegaya et al. (2012) were adopted.

## 3 Experimental Set-up

### 3.1 Rough and Smooth Surfaces

The experimental conditions were designed to separate the roughness effect on the transfer coefficients into two factors: (1) the aerodynamic effect of the blocks causing a momentum deficit, and (2) partitioning of a scalar boundary layer above a wet street surface because of dry blocks. Furthermore, the effect of the streamwise length of the street source area was examined. Figure 1 shows three types of configurations used for the estimation of the scalar transfer coefficients: (i) dry cubical staggered arrays located on a wet surface, hereafter called 'ST1', identical to array ST1 used in Hagishima et al. (2009) and Ikegaya et al. (2012); (ii) smooth wet surfaces with dry square patches (hereafter 'ST0'); and (iii) a wet smooth surface (hereafter 'Smooth'). The linear dimension of the dry cubes and dry patches is fixed at 25 mm (hereafter $L$). As shown by the grey-shaded areas in Fig. 1, a wet street surface of the ST1 array is a scalar source, thus, dry blocks act not only to reduce the airflow but also to disturb the internal scalar boundary layer over a wet street. In contrast, the wet surface of the ST0 array is partitioned with small dry square patches with the same sized cubes as the ST1 array.

Three conditions of plan-area density for blocks ($\lambda_{p\text{-block}}$) and dry patches ($\lambda_{p\text{-patch}}$), 7.7, 17.4, and 30.9 %, are adopted for the ST1 and ST0 arrays, and the scalar transfer coefficients for a total of seven cases, including the Smooth case, were estimated. The values of $\lambda_{p\text{-block}}$ and $\lambda_{p\text{-patch}}$ can be calculated from $\lambda_p = L^2/(W+L)^2$, where $L$ is the length of a dry block and a dry patch, and $W$ is the spacing between blocks or patches (see Fig. 2d–f).

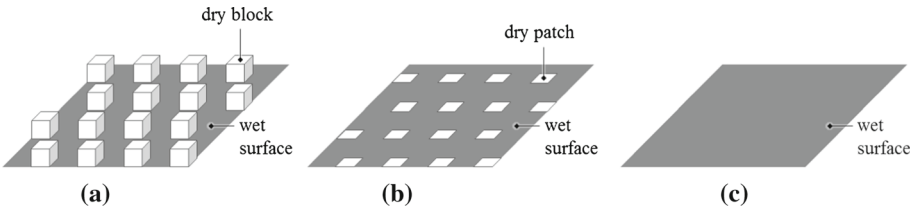


**Fig. 1** Three types of configurations, indicating **a** cubical staggered arrays with wet streets (ST1), **b** smooth wet surfaces with dry square patches (ST0), and **c** a wet smooth surface (Smooth)

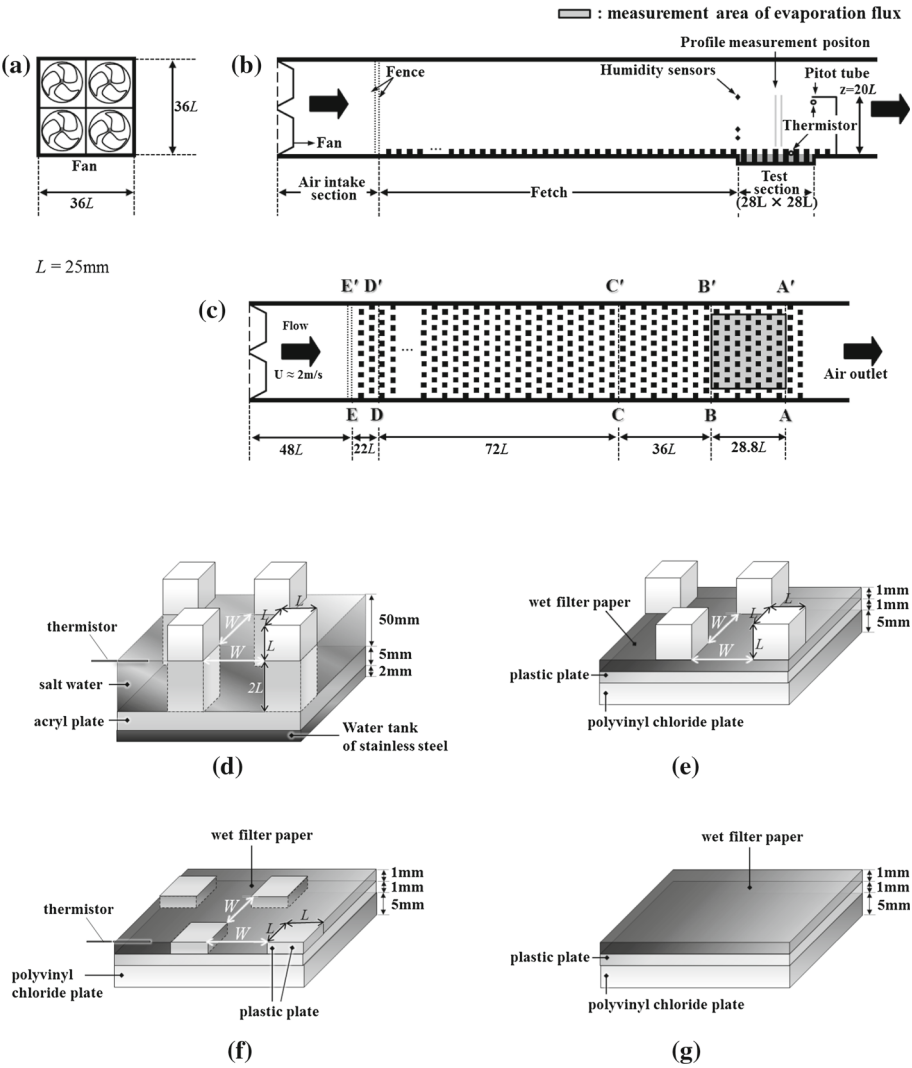


**Fig. 2** Schematic diagrams of the arrangement of target surfaces in an open-type wind-tunnel, indicating **a** four propeller fans, **b** elevation view, **c** plan view, showing street units used for the measurement of evaporation, indicating **d** the cube array ST1 installed in a water tank for the salinity method, **e** the cube array ST1 installed in the fetch area as an extended scalar source, **f** a wet smooth surface with dry patches ST0, and **g** smooth

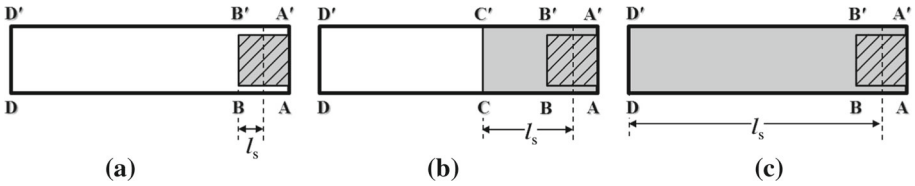


**Fig. 3** Allocation of scalar source area, **a** smallest size condition ($l_s = 14.4L$), **b** medium size condition ($l_s = 50.4L$), and **c** largest size condition ($l_s = 122.4L$). *Grey areas* indicate areas containing wet surface; *shaded portion* refers to target area of measurement of the evaporation

### 3.2 Wind-Tunnel Device and Arrangement of Rough and Smooth Walls

An open-ended blow-down type wind tunnel with a total length of 6 m was used, the same as that used by Ikegaya et al. (2012). The interior cross-section of the tunnel had a constant width of 0.9 m and height of 0.9 m, as shown in Fig. 2a–c. The tunnel consists of an air-intake section, an upwind area with a streamwise length of 3.25 m ($130L$) between lines EE′ and BB′ (Fig. 2b; hereafter referred to as the 'fetch section'), and a test section between lines BB′ and AA′. At the intake section, two mesh screens are installed to adjust the uniformity of the inflow generated by four forced draft fans. In contrast, the test section includes a square-shaped target area of $28.8L \times 28.8L$ for the measurement of evaporation.

The floor surface of the fetch section has the same geometry as the test section to obtain the continuous development of the momentum boundary layer from the upwind edge EE′ to the test section. With regard to the scalar boundary condition of the fetch section, we adopted three different conditions for the allocation of scalar source for each case, as illustrated in Fig. 3. The condition of the smallest scalar source area is shown in Fig. 3a, where only the test section includes a wet surface, and the upwind region of the test section is completely dry. Another condition is the largest scalar source area shown in Fig. 3c, where both the test section and the whole fetch section between lines DD′ and AA′ comprise a wet surface, and the last condition is the medium scalar source size shown in Fig. 3b. Hereafter, we identify the streamwise length as the distance between a leading edge of scalar source and the centre of the test section '$l_s$'. The extended scalar source area in the fetch section was simulated using wet filter papers (Fig. 2e–g).

In the present study, the name of each condition is determined by the surface geometry of the test section (i.e. ST1, ST0, and Smooth) and the size of the scalar source (i.e. small S for $l_s = 14.4L$, medium M for $l_s = 50.4L$, and large L for $l_s = 122.4L$) using simplified forms, for instance, 'ST1-S'. The details of all cases are listed in Table 1.

### 3.3 Instrumentation and Measurement Methods

We used two methods to measure the evaporation, including the salinity method used by Ikegaya et al. (2012) for both ST1 and Smooth arrays, and the water evaporation method used by Narita (2007) for the ST0 array.

In the salinity method, a tank with a $28.8L$ square base and $2L$ depth filled with saline water was embedded in the test section as shown in Fig. 2b, d, and the amount of evaporation from the saline water surface was determined based on the increases in water salinity over a period of 2 h under constant flow conditions. The water salinity was measured with a salinometer (Guildline Instruments, Autosal 8400B), with calibration carried out using the International Association for the Physical Sciences of the Ocean seawater standard every 24 h. Details of the measurement procedure and the validity are given in Ikegaya et al. (2012).

**Table 1** Details of rough and smooth surfaces used in experiments

| Surfaces | $\lambda_{\text{p-block/patch}}$ (%) | $W$ | $l_s$ | Remarks |
|---|---|---|---|---|
| ST1-S * | 7.7, 17.4, 30.9 | $2.6L$, $1.4L$, $0.8L$ | $14.4L$ | Staggered array of dry cubes with of size $L$ (25 mm) on a wet street surface |
| ST1-M | 7.7, 17.4, 30.9 | $2.6L$, $1.4L$, $0.8L$ | $50.4L$ | |
| ST1-L | 7.7, 17.4, 30.9 | $2.6L$, $1.4L$, $0.8L$ | $122.4L$ | |
| ST0-S | 7.7, 17.4, 30.9 | $2.6L$, $1.4L$, $0.8L$ | $14.4L$ | Smooth wet surface with dry square patches of size $L \times L$ arranged in staggered layout |
| ST0-M | 7.7, 17.4, 30.9 | $2.6L$, $1.4L$, $0.8L$ | $50.4L$ | |
| ST0-L | 7.7, 17.4, 30.9 | $2.6L$, $1.4L$, $0.8L$ | $122.4L$ | |
| Smooth-S | 0 | $\infty$ | $14.4L$ | Smooth wet surface |
| Smooth-M | 0 | $\infty$ | $50.4L$ | |
| Smooth-L | 0 | $\infty$ | $122.4L$ | |

$\lambda_{\text{p-block/patch}}$: ratio of block plan-area for ST1 or dry patches for ST0 to total floor area
$W$: spacing between dry patches (see Fig. 2d–f)
$l_s$: streamwise length of area with wet surface (see also Fig. 3)
*: data from Ikegaya et al. (2012)

In the water evaporation method, wet filter papers glued to flat plastic plates were installed on the wind-tunnel floor of the test section (see Fig. 2e–g), and the evaporation was calculated from the difference in the mass of the wet filter papers before and after the time period of 2 h while the test section was exposed to a constant airflow. This mass was measured using a mass balance (A&D, EP-60KA) with an accuracy of 0.001 kg.

During the time period of the exposure to constant airflow in the salinity method and the water evaporation method, wind speed, air temperature, relative humidity above the test section, and the surface temperature of wet surfaces were recorded every 30 s. Based on the measurements, the scalar transfer coefficient per unit wet area $C_{\text{E wet}}$ defined by Eq. 8 was calculated for each case, as in Ikegaya et al. (2012),

$$C_{\text{E wet}} = \frac{E_{\text{wet}}}{\rho u_{\text{ref}} \left(q_{\text{surf}} - q_{\text{ref}}\right)}, \tag{8}$$

where $E_{\text{wet}}$ is the evaporation rate per wet area (kg m$^{-2}$s$^{-1}$). The reference wind speed $u_{\text{ref}}$ and reference specific humidity $q_{\text{ref}}$ were determined as values at a height of $20L$. In addition, the scalar transfer coefficient per unit lot-area, including both wet and dry surfaces $C_{\text{E lot}}$, was estimated from

$$C_{\text{E lot}} = \frac{E_{\text{lot}}}{\rho u_{\text{ref}} \left(q_{\text{surf}} - q_{\text{ref}}\right)}, \tag{9}$$

where $E_{\text{lot}}$ is the evaporation of the whole of the test section (kg m$^{-2}$s$^{-1}$) and $E_{\text{lot}} = E_{\text{wet}} \left(1 - \lambda_{\text{p}}\right)$.

The reference wind speed was measured using a pitot-static tube at a height of $20L$ above the leeward edge of the test section, and maintained at approximately 1.9−2 m s$^{-1}$ for all measurements; the Reynolds number based on the reference velocity and the block height was about 3300. In contrast, the air temperature at the reference height of $20L$ was measured

using a thermistor thermometer (TechnolSeven, DS101) with an accuracy of 0.1°C, with the absolute humidity of the air above the test section measured at three heights ($5L$, $10L$, and $20L$) at the centre of the line B-B′ (Fig. 2b) using hygrometers (Sensirion, SHT75) with an accuracy of ±1.8 %.

Furthermore, the temperature of the wet surfaces of the measurement target of the evaporation was measured so as to determine the saturated specific humidity on the wet surface using three thermistor thermometers on the lateral centre line of the test section at intervals of about 150 mm. In the salinity method, the thermometers were floated on the water surface, whereas they were inserted into the middle of the wet filter papers in the water evaporation method. The variation of the temperature at the three positions was less than 0.2 °C, and averaged values of the three sensors were used for the analysis.

All measurements for each case were conducted at least three times, and the average of the scalar transfer coefficients derived using Eqs. 8 and 9 was used for the subsequent analysis. The variation in estimated transfer coefficients was <4 %.

### 3.4 Inflow Conditions of Wind-Tunnel

Prior to the main experiment to measure the evaporation rate, we obtained the vertical profiles of the streamwise velocity component over the Smooth and ST1 arrays with $\lambda_{\text{p-block}} = 17$ %. Because of the limitation of the experimental conditions and devices, we used a system consisting of a pitot tube (with a total pressure hole diameter of 1.5 mm) and a differential manometer (DMP 201N12, Okano Works) with an accuracy of 0.02 Pa for this measurement instead of hot-wire anemometry. It is thus difficult to precisely analyze the turbulent statistics due to the slow response time of the measurement system, which included a tube connecting the pitot tube to the manometer. The measurement was performed at the positions located on a spanwise line near the centre of the test section shown in Fig. 4a. The measurement sampling frequency and time period were 10 Hz and 300 s, respectively. The results are

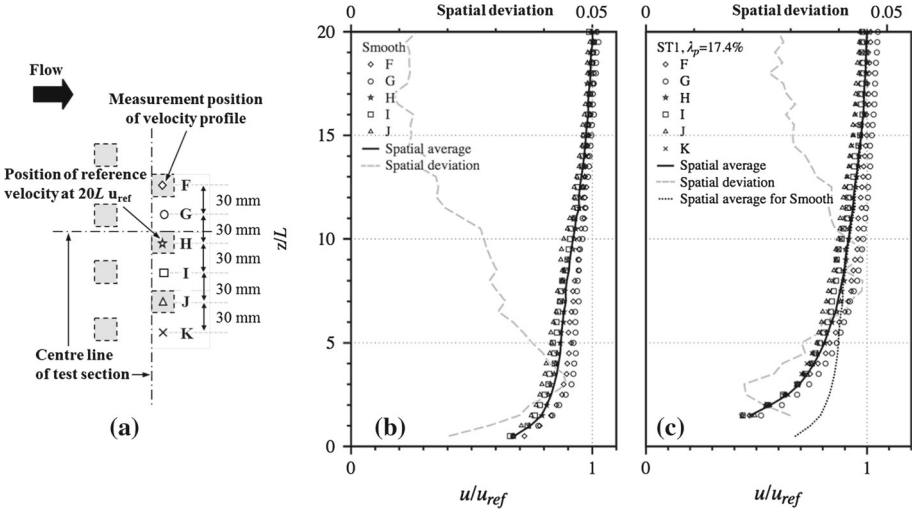


**Fig. 4** Measurement positions of the velocity profiles (**a**), normalized mean velocity profiles for a smooth surface (**b**), and for cube array ST1 with $\lambda_{\text{p-block}} = 17.4$ % (**c**). *Lines* (in **b**, **c**) indicate the spatial average of each positions (F–K) at the same height, *broken lines* (in **b**, **c**) indicate spatial deviation of each positions (F–K) at the same height, and *dot lines* (in **c**) indicate the spatial average of the Smooth case for the comparison

shown in Fig. 4b, c, with velocity normalized by a value at a height of $20L$ above a centred cube (see Fig. 4a).

The mean velocity magnitudes of both Smooth and ST1 arrays show the difference due to the spanwise positions at each height, which is unfortunately caused by the non-uniformity of the inflow of this wind-tunnel. The values at position G are mostly the smallest among the five positions, and as the position moves from left to right viewed from the upwind side, the speed increases slightly. The spatial variations of the mean velocity magnitude of the 40 heights normalized by the reference velocity are in the range from 1 to 4.5 % for the Smooth case, and from 2 to 4.5 % for the ST1 array. This spatial variation becomes large with the increase of the height up to $3L$ and $10L$ for Smooth and ST1 arrays, respectively, and gradually decreases.

The spatially-averaged mean profiles of the Smooth and ST1 arrays show almost equivalent steep gradients above approximately $8L$. In contrast, below a height of $8L$, the profile of the ST1 array shows a departure from data of the Smooth case, and gradually increases the velocity gradient because of the larger shear generated by the underlying cube array. The profile of the Smooth case shows a larger gradient below approximately $2L$ compared to above this layer, and the spatial variation of this lower layer is smaller than the upper remaining layer. Although further discussion based on the turbulent statistics is not possible because of the low frequency response of the present measurement system, the height about $5L$ to $8L$, where spatially-averaged mean profiles show a departure from the Smooth and ST1 arrays, might be associated with the boundary-layer height of the ST1 array. Hagishima et al. (2009) reported that the momentum boundary-layer height of array ST1 ($\lambda_{\text{p-block}} = 17$ %) determined by a negative peak of the skewness of the streamwise velocity is $7.5L$ under the same conditions of the length of the fetch section and geometry of the block arrays, although they used a different wind tunnel. Based on this result, the reference heights $20L$ for velocity and specific humidity used to determine $C_{\text{E lot}}$ and $C_{\text{E wet}}$ is supposed to be far above the momentum boundary layer generated by an underlying surface.

The spanwise uniformity of the inflow of this self-built wind tunnel is not small compared with those of ordinary wind tunnels, and this problem might be caused by the relatively short intake section. However, in spite of such a limitation, it is supposed that the flow close to the wall surfaces over the test section is well adjusted, and reaches equilibrium with the underlying topography because of the fetch of $130L$, based on previous studies. For example, the data shown in Cheng and Castro (2002) indicate that the top of the inertial sublayer over a staggered cube array exists at around three times the cube size at the streamwise fetch of about $130L$. Similarly, Hagishima et al. (2009) estimated the location of the inertial sublayer for the ST1 array ($\lambda_{\text{p}} = 17$ %) as from $2.0L$ to $3.5L$ in height under the same conditions of the fetch for this experiment. Since the objective of the measurements is to estimate the spatially-averaged evaporation of the test section, which is on the lee side of the long fetch section, and to examine the effects of the topography and the scalar source allocation, we believe that the inflow condition of the present experiment is acceptable.

## 4 Results and Discussion

### 4.1 Relationship Between Scalar Transfer Coefficients and Fraction of Dry Patches/Blocks

Figure 5 shows the scalar transfer coefficients $C_{\text{E wet}}$ defined by the evaporation rate of the wet areas of the three configurations under the condition of the largest and smallest scalar source

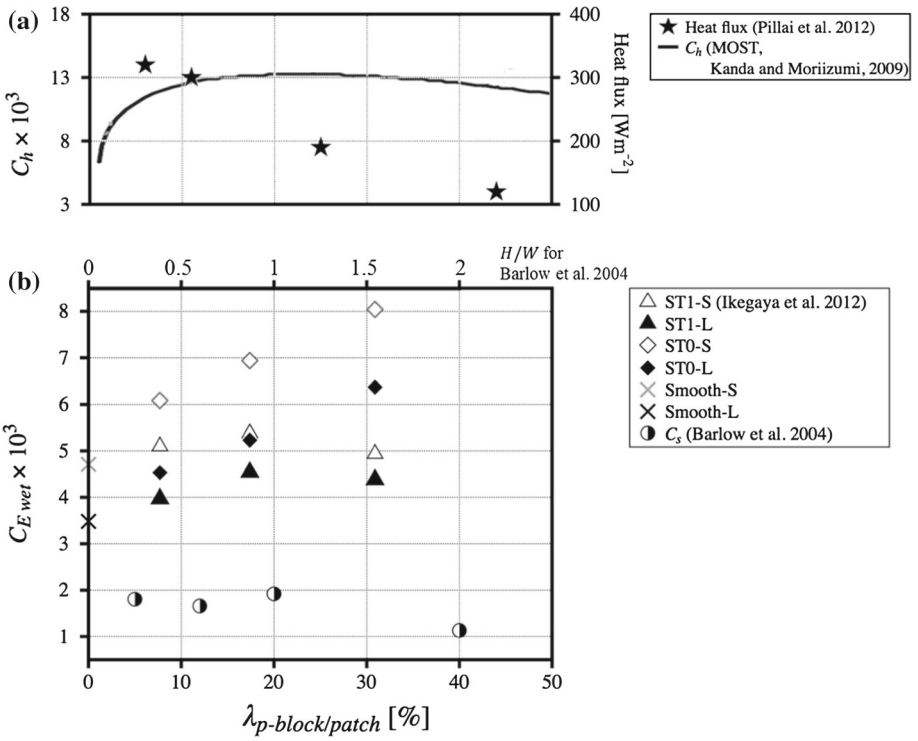


**Fig. 5** Scalar transfer coefficients for the present experiment with relevant past data under the various block/patch plan-area ratio conditions: **a** heat transfer coefficients $C_h$ for the staggered cube arrays shown in Kanda and Moriizumi (2009), estimated $C_h$ for block arrays based on the $Re^* - B^{-1}$ relation and roughness length $z_o$ derived from Macdonald's model, and heat fluxes for street surfaces of block arrays given in Pillai and Yoshie (2012), **b** scalar transfer coefficients based on the evaporation over wet areas $E_{wet}$ for street surfaces of block arrays obtained in the present experiment under conditions of maximum source area ($l_s = 122.4L$), white triangles indicate the data of the ST1-S array from Ikegaya et al. (2012), and *half-filled circles* indicate transfer coefficients $C_s$ for canyon facets of street from Barlow et al. (2004)

area. The horizontal axis is the plan-area ratio of blocks $\lambda_{p\text{-block}}$ and dry patches $\lambda_{p-patch}$; the plot at $\lambda_{p\text{-block/patch}} = 0$ % refers to a fully-wet Smooth case. The data for the ST1-S array with the minimum scalar source size obtained by Ikegaya et al. (2012) and transfer coefficients of a street with 2D canyon obtained by Barlow et al. (2004) are also included for reference. The scalar source in the data of Barlow et al. (2004) was only allocated in a street of the measurement target. The previous work by Pillai and Yoshie (2012) for the heat transfer process over cube arrays is also shown in Fig. 5a for comparison. As mentioned in Sect. 2, the data of Pillai and Yoshie (2012) were derived from RANS simulations for cube arrays with an approximately uniform heat source, and the boundary conditions of the temperature of the inflow and surfaces of the block arrays were determined based on their wind-tunnel experiment. The data shown in the figure refer to the convective heat transfer per unit street area. Since the thermal conditions of the inflow and surfaces were almost similar among their four cases, the data of heat flux can be treated as comparable information to our $C_{E\,wet}$. The estimation of $C_h$ by Kanda and Moriizumi (2009) included in Fig. 5a is based on Macdonald's $z_o$ model and an exponential relation between $\kappa B^{-1}$ and $Re^*$ for staggered cube arrays.

As expected, the data of $C_{\mathrm{E\,wet}}$ for smooth surfaces (ST0-L and Smooth-L arrays) show a monotonic increase against $\lambda_{\mathrm{p\text{-}patch}}$, and this increasing trend is approximately linear. This is because dry patches partition the internal scalar boundary layer over wet surfaces, producing a thinner scalar boundary layer, and enhancing scalar transport. The value of $C_{\mathrm{E\,wet}}$ for the ST0-L array with $\lambda_{\mathrm{p\text{-}patch}} = 31$ % is about 1.8 times that of the Smooth-L array (a fully wet, smooth condition). In contrast, the data for the ST1-L array exhibit a positive peak against $\lambda_{\mathrm{p\text{-}block}}$, although the number of plots is only four, including the Smooth data, and all the ST1-L array data values are greater than that for the Smooth case. This tendency is qualitatively similar to that of the ST1-S array presented by Ikegaya et al. (2012). The data for a 2D street reported by Barlow et al. (2004) under a single source condition also exhibit a positive peak at a street-aspect ratio of $H/W = 1$, although a precise comparison of the condition for the peak between our 3D canopy and their 2D canopy cannot be made. In contrast, the results of Pillai and Yoshie (2012) under approximately uniform scalar source conditions (i.e. the entire surfaces of blocks and streets form the scalar source) show a monotonic decrease and are completely inconsistent with the other experiments.

As mentioned before, Ikegaya et al. (2012) suggested that the positive peak of $C_{\mathrm{E\,wet}}$ against $\lambda_{\mathrm{p\text{-}block}}$ is caused by two contrasting aerodynamic mechanisms: (i) decreased horizontal advection due to a block array, and (ii) enhanced vertical turbulent mixing due to vortices around blocks. However, considering the significant increase in $C_{\mathrm{E\,wet}}$ of the ST0 array against $\lambda_{\mathrm{p\text{-}patch}}$, the heterogeneous distribution of a wet surface, i.e. the destruction of the scalar boundary layer by dry blocks, is supposed to be the third important factor behind the positive peak of $C_{\mathrm{E\,wet}}$ against $\lambda_{\mathrm{p\text{-}block}}$ shown in the present experiment. Since the size and spacing of dry blocks of the ST1 array are equivalent to those of the dry patches of the ST0 array, the subtraction of $C_{\mathrm{E\,wet}}$ of the ST1 array from that of the ST0 array for each $\lambda_{\mathrm{p\text{-}block}}$ condition, namely $0.6 \times 10^{-3}$ for $\lambda_{\mathrm{p\text{-}block}} = 8$ %, $0.7 \times 10^{-3}$ for $\lambda_{\mathrm{p\text{-}block}} = 17$ %, and $2.0 \times 10^{-3}$ for $\lambda_{\mathrm{p\text{-}block}} = 31$ %, can be interpreted as the genuine aerodynamic effect of the blocks. In other words, block arrays aerodynamically work only to reduce the scalar transfer efficiency for all conditions of block density, and this effect increases with $\lambda_{\mathrm{p\text{-}block}}$, in particular between 17 and 31 %. This condition of $\lambda_{\mathrm{p\text{-}block}}$ from 17 to 31 % is consistent with that for the transition of the canopy-flow regime suggested by Hagishima et al. (2009). They indicated that the drag coefficient starts to decrease for staggered cube arrays because of the change of the canopy-flow features from wake interference to skimming in terms of the reduction of total surface drag. The positive peaks shown in the present data and Barlow et al. (2004) might be a consequence of the superposition of two contrasting trends against block density $\lambda_{\mathrm{p\text{-}block}}$: the first is the enhancement of evaporation due to the scalar source partitioning of dry obstacles, and the other is the decrease of horizontal advection due to the aerodynamic effect of the blocks. The reason the data of Pillai and Yoshie (2012) have no peak but a monotonic decrease against $\lambda_{\mathrm{p\text{-}block}}$ might be associated with the thermal boundary conditions of their simulation, which reproduce uniformly heated rough surfaces with no scalar partitioning effect. It is noteworthy that the simple estimation of $C_{\mathrm{h}}$ given by Kanda and Moriizumi (2009) based on the roughness length $z_{\mathrm{o}}$ and the $Re^* - B^{-1}$ relationship exhibits a convex curve (see Fig. 5a), and this trend is inconsistent with the feature of block arrays uniformly covered by a scalar source.

With regard to the comparison between ST1-L and ST1-S, although they show similar tendencies, a slight difference is apparent. The $C_{\mathrm{E\,wet}}$ values of the ST1-L array for $\lambda_{\mathrm{p\text{-}block}} = 31$ % are larger than for $\lambda_{\mathrm{p\text{-}block}} = 8$ %. In contrast, the data for the ST1-S array show the opposite trend, implying that the relationship between $C_{\mathrm{E\,wet}}$ and the block density is, to some extent, affected by the condition of the scalar source size. In addition, the difference between ST1-S and ST1-L gradually becomes small with $\lambda_{\mathrm{p\text{-}block}}$. In contrast, the difference

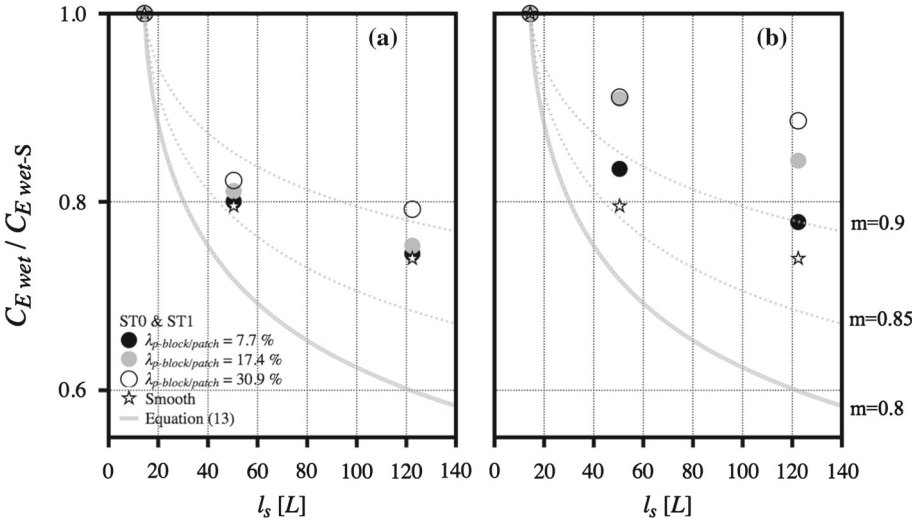


**Fig. 6** The decreasing ratio of $C_{\mathrm{E\,wet}}$ for the ST0 array, and **a** for the ST1 array and **b** with the length of the upwind scalar area characterized by $l_{\mathrm{s}}$, where *black circles* indicate $\lambda_{\mathrm{p\text{-}block/patch}} = 7.7$ %, *grey circles* indicate $\lambda_{\mathrm{p\text{-}block/patch}} = 17.4$ %, *white circles* indicate $\lambda_{\mathrm{p\text{-}block/patch}} = 30.9$ %, and stars (in 6a and 6b) indicate the case of the Smooth array. The *lines* indicate the estimated values of a smooth surface expressed by Eq. 13 when m = 0.8 (*solid grey line*), $m = 0.85$ and 0.9 (*dotted grey lines*) for reference

in $C_{\mathrm{E\,wet}}$ between arrays ST0-S and ST0-L is much larger than between arrays ST1-S and ST1-L, and the difference is almost constant for all the $\lambda_{\mathrm{p\text{-}patch}}$ conditions, including the fully wet Smooth case. Let us speculate about how $C_{\mathrm{E\,wet}}$ behaves if $\lambda_{\mathrm{p\text{-}block/patch}}$ increases more than in the present conditions, and reaches 100 %. In the case of a smooth surface ST0, a wet area, i.e. marginal area of dry patches, is stretched and always comprises a network with a staggered shape regardless of the ratio of dry patch area $\lambda_{\mathrm{p\text{-}patch}}$. Thus, the effect of the upwind length of the scalar source area might remain, and show a similar difference in $C_{\mathrm{E\,wet}}$ between arrays ST0-L and ST0-S up to relatively high $\lambda_{\mathrm{p\text{-}patch}}$ conditions, and after that, the difference probably diminishes gradually. In contrast, a wet street network surrounded by blocks of ST1 is exposed to the highly complex canopy flow, and such a turbulent canopy flow might work to reduce the effect of the upwind source area characterized by $l_{\mathrm{s}}$ under relatively low $\lambda_{\mathrm{p\text{-}block}}$ conditions, and the difference in $C_{\mathrm{E\,wet}}$ between arrays ST1-S and ST1-L may disappear, as partly suggested in Fig. 5b.

### 4.2 Effect of Upwind Scalar Source on Scalar Transfer Coefficients

Figure 6 indicates how the scalar transfer coefficients decrease with the length of the upwind scalar area characterized by $l_{\mathrm{s}}$; the vertical axis is $C_{\mathrm{E\,wet}}$ divided by a value for case S with the minimum scalar source area. Curves included are derived from a relation between the local Nusselt number, $Nu_x$, Reynolds number, $Re_x$, and Prandtl number $Pr$ for turbulent forced convection over a flat plate with a uniform surface temperature, as follows.

According to Incropera and DeWitt (2002),

$$Nu_x = 0.0296\, Re_x^m\, Pr^{1/3}, \tag{10}$$

where $m = 0.8$, $Nu_x = hx/\lambda$, $Re_x = u\,x/\nu$, $Pr = \nu/\alpha$, $\lambda$ denotes the heat conductivity (W m$^{-1}$K$^{-1}$), $x$ refers to the distance from the upwind edge of the plate (m), $\alpha$ is the thermal

diffusivity ($m^2 s^{-1}$). Based on the assumption of the analogy between heat transfer and mass transfer, Eq. 10 can be modified as

$$Sh_x = 0.0296\, Re_x^m\, Sc^{1/3}, \tag{11}$$

where the local Sherwood number $Sh_x = k\,x/\rho\,D$, the Schmidt number $Sc = \nu/D$, and $D$ is the vapour diffusivity ($m^2 s^{-1}$).

Since the measured $C_{\mathrm{E\,wet}}$ in the present study represents the spatially-averaged transfer speed for the test section, Eq. 11 was modified by integration of $x$ between $l_s - 0.5\,l_{\mathrm{test}}$ and $l_s + 0.5\,l_{\mathrm{test}}$, where $l_{\mathrm{test}}$ is the streamwise length of the test section, to give

$$\overline{Sh} = 0.037\, Re_{ls}^m\, Sc^{1/3}\, f(\chi), \tag{12}$$

where $\overline{Sh}$ is the area average for the test section, $Re_{ls}$ is the Reynolds number defined by the length $l_s$, $f(\chi) = \left\{\left(1 + 0.5\chi^{-1}\right)^m - \left(1 - 0.5\chi^{-1}\right)^m\right\}\chi$, and $\chi = l_s/l_{\mathrm{test}}$. Equation 12 gives the estimation of $C_{\mathrm{E}}$ as an area-average equivalent to the present measurement as follows,

$$\overline{C_{\mathrm{E}}} = 0.037\, Re_{ls}^{m-1}\, Sc^{-\frac{2}{3}}\, f(\chi). \tag{13}$$

The data for the fully wet Smooth case show a gradual decrease compared with the estimation of Eq. 13 with $m = 0.8$, and the plots range between curves with $m = 0.85$ and 0.9. The decreasing of $C_{\mathrm{E\,wet}}$ for the ST0 array is similar to that of the Smooth array, and cases with a high dry-patch ratio $\lambda_{\mathrm{p\text{-}patch}}$ indicate a smaller reduction. This trend indicates that the length scale $l_s$ tends to overestimate the effect of streamwise scalar source size for a surface of the ST0 array with high $\lambda_{\mathrm{p\text{-}block}}$ conditions, which is partly covered by a dry area, and is plausible.

The decreasing rate of $C_{\mathrm{E\,wet}}$ for cubical arrays ST1 is much smaller than that for smooth surfaces (Smooth and ST0). This might be due to the scalar source partitioning of dry blocks but also the aerodynamic effect characterized by complex canopy flow.

### 4.3 Scalar Transfer Coefficients Defined by Lot-Area

Figure 7 shows the scalar transfer coefficients $C_{\mathrm{E\,lot}}$, which are defined by the evaporation flux per lot-area of the three configurations under the condition of the largest scalar source area. The data for smooth surfaces, including the Smooth case and ST0 array, increase significantly from $\lambda_{\mathrm{p\text{-}patch}}$ = zero to 8 %, and this increasing trend becomes mild for $\lambda_{\mathrm{p-patch}}$ from 8 to 31 %. In contrast, $C_{\mathrm{E\,lot}}$ for cube arrays including Smooth and ST1 arrays shows a weak increase up to $\lambda_{\mathrm{p\text{-}block}}$ of 17 %, and decreases at $\lambda_{\mathrm{p\text{-}block}}$ of 31 %. These results clearly show the oasis effect of wet areas surrounded by dry patches and dry blocks, where the spatially-averaged evaporation rate per unit lot-area exceeds that of a fully wet surface area. As previous flux measurements in a real urban setting (e.g. Moriwaki and Kanda 2004) and outdoor experiments (e.g. Hagishima et al. 2007) have shown, it is possible that the surface energy balance in urban areas, which are mostly covered by artificial dry materials, shows relatively large evaporation for their low green coverage ratios. If we increase the condition of $\lambda_{\mathrm{p\text{-}patch}} > 31$ %, the effect of the decrease in wet-area ratio gradually exceeds the enhanced evaporation due to dry patches, and $C_{\mathrm{E\,lot}}$ decreases below the value of a fully wet condition, and will finally drop to zero. From the viewpoint of the application in urban planning to utilize vegetation for environmental mitigation, it might be interesting to determine the conditions of $\lambda_{\mathrm{p\text{-}patch}}$ where $C_{\mathrm{E\,lot}}$ becomes equivalent to the fully wet condition. Nevertheless, considering the fact that the oasis effect shown in Fig. 7 is due to the enhanced evaporation in small

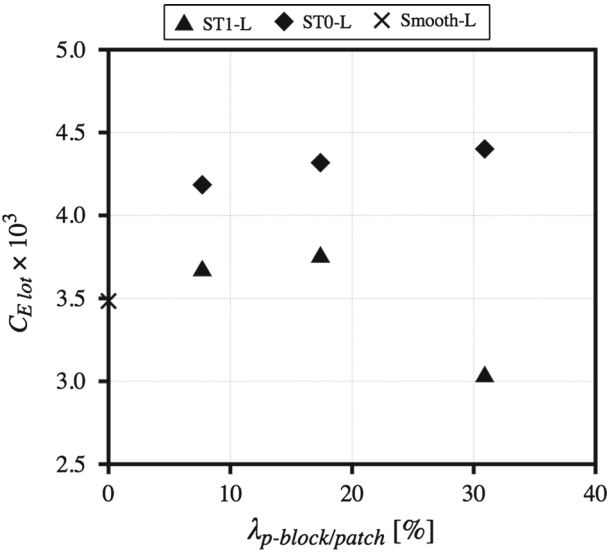


**Fig. 7** Scalar transfer coefficient based on evaporation over the entire lot-area $E_{\mathrm{lot}}$ under the maximum source area conditions ($l_{\mathrm{s}} = 122.4L$)

wet areas partitioned by dry patches of 25 mm linear size, as expressed by the exponential relationship between $Sh_x$ and $Re_x$ (see Eq. 11), the relationship between $\lambda_{\mathrm{p\text{-}patch}}$ and $C_{\mathrm{E\,lot}}$ will depend on the size of each wet patch.

### 4.4 Effects of Scalar Source Partitioning and Roughess on Parameter $B^{-1}$

Based on the similarity theory expressed by Eqs. 1 and 3, parameter $B$ defined by Eq. 4 can be modified as follows,

$$B^{-1} = \frac{1}{\kappa}\ln\left(\frac{z_{\mathrm{o}}}{z_{\mathrm{os}}}\right) = \frac{1}{\kappa}\ln\left(\frac{z}{z_{\mathrm{os}}}\right) - \frac{1}{\kappa}\ln\left(\frac{z}{z_{\mathrm{o}}}\right) = \frac{q_{\mathrm{surf}} - q}{q_*} - \frac{u}{u_*}$$
$$= Da_0^{-1} - C_{\mathrm{m}}^{-0.5}. \tag{14}$$

As an approximation of $B^{-1}$, we calculated $C_{\mathrm{E}}^{*-1} - C_{\mathrm{m}}^{*-0.5}$ (hereafter we call it $B'^{-1}$) based on the measurements, where the transfer coefficients, for scalar $C_{\mathrm{E}}^*$ and momentum $C_{\mathrm{m}}^*$, are defined as

$$C_{\mathrm{E}}^* = \frac{E_{\mathrm{lot}}}{\rho\, u_*\,(q_{\mathrm{surf}} - q_{\mathrm{ref}})}. \tag{15}$$

$$C_{\mathrm{m}}^* = \frac{u_*^2}{u_{\mathrm{ref}}^2}. \tag{16}$$

Note that these transfer coefficients $C_{\mathrm{E}}^*$ and $C_{\mathrm{m}}^*$ are similar to the interfacial Dalton number $Da_0$ included in Eq. 14 and the drag coefficient $C_{\mathrm{m}}$ defined by Eq. 2, respectively, although they are not exactly the same; the reference specific humidity $q_{\mathrm{ref}}$ in $C_{\mathrm{E}}^*$ is defined by a value above the boundary layer at $20L$, other than the upper boundary of the interfacial sublayer. Similarly, $u_{\mathrm{ref}}$ in Eq. 16 is determined by the reference velocity at a height of $20L$ far above the logarithmic layer in this study.

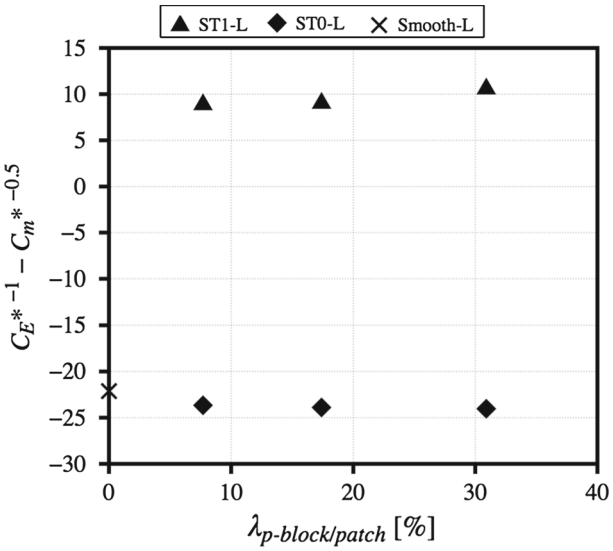


**Fig. 8** Estimated $B'^{-1}(= C_{\mathrm{E}}^{*-1} - C_{\mathrm{m}}^{*-0.5})$ based on data of maximum source area conditions ($l_{\mathrm{s}} = 122.4L$)

The friction velocity $u_*$ for cube arrays ST1 was calculated from the drag coefficients of block arrays with the same geometry and streamwise length as shown in Hagishima et al. (2009). In contrast, $u_*$ for smooth surfaces was newly measured based on a floating drag balance method in another return-type wind-tunnel; the measurement procedure and instrumentation are exactly the same as Hagishima et al. (2009).

Figure 8 shows the estimated $B'^{-1}(= C_{\mathrm{E}}^{*-1} - C_{\mathrm{m}}^{*-0.5})$ against the plan-area ratio $\lambda_{\mathrm{p\text{-}block/patch}}$ under the maximum scalar source conditions. $B'^{-1}$ for the smooth surfaces (Smooth case and ST0 array) is negative, and decreases with the increase in the fraction of dry patches $\lambda_{\mathrm{p\text{-}patch}}$. Because of the same surface geometry of both ST0 and Smooth arrays, it is obvious that $z_{\mathrm{o}}$ for these four conditions is equivalent. Therefore, the decreasing trend of $B'^{-1}$ for the ST0 array suggests the scalar roughness length significantly increases because of the heterogeneous distribution of the scalar source, which impedes the continuous development of the scalar boundary layer. Since the coefficients $C_{\mathrm{E}}^*$ and $C_{\mathrm{m}}^*$ shown in Fig. 8 are determined by specific humidity and velocity far above the boundary layer, other than those within the interfacial sublayer, we cannot treat $B'^{-1}$ as $\kappa^{-1} \ln(z_{\mathrm{o}}/z_{\mathrm{os}})$, however, the negative values of $B'^{-1}$ for the ST0 array imply (the possibility) that the spatial distribution of the scalar source results in larger $z_{\mathrm{os}}$ compared to $z_{\mathrm{o}}$. In contrast, all values of $B'^{-1}$ for rough surfaces (ST1) are much larger than for the Smooth case, and $B'^{-1}$ shows a slight increase as $\lambda_{\mathrm{p-block}}$ increases, especially from $\lambda_{\mathrm{p-block}} = 17$ to 31 %. This implies that $z_{\mathrm{o}}$ of the present block arrays is much larger than $z_{\mathrm{os}}$, and the ratio of $z_{\mathrm{o}}$ to $z_{\mathrm{os}}$ varies with topography in spite of their similar $Re^*$ conditions.

## 5 Conclusions

The present study reports the results of a wind-tunnel experiment on the evaporation from smooth and rough surfaces, including wet street surfaces of cube arrays, wet smooth surfaces

with dry patches, and fully wet smooth surfaces. The experimental data were transformed into scalar transfer coefficients $C_{\mathrm{E\,wet}}$ and $C_{\mathrm{E\,lot}}$, defined as the flux per source area and lot-area, and the effect of the topography and the allocation of scalar source area were extensively discussed.

It has been widely known that the aerodynamic roughness length $z_{\mathrm{o}}$ and drag coefficient $C_{\mathrm{m}}$ of block arrays show a convex trend against the block plan-area $\lambda_{\mathrm{p\text{-}block}}$ in accordance with the canopy flow regime, namely isolated flow, wake interference flow, and skimming flow. Similarly, Barlow et al. (2004) and Ikegaya et al. (2012) presented a convex trend of scalar transfer coefficients $C_{\mathrm{E\,wet}}$ of a street surface of block arrays against $\lambda_{\mathrm{p\text{-}block}}$. However, the present study suggests that the positive peak of the $C_{\mathrm{E\,wet}} - \lambda_{\mathrm{p\text{-}block}}$ relationship shown in these two experiments is a consequence of the superposition of two opposite factors, namely the enhancement of transport due to the partitioning of the scalar boundary layer by block surfaces with no scalar source, and the reduction of advection due to block arrays. In the case of block arrays, whole surfaces that include blocks and streets work as a scalar source, and the $C_{\mathrm{E\,wet}}$ values for street surfaces of block arrays show a monotonic decrease against $\lambda_{\mathrm{p\text{-}block}}$ because of the reduction of wind speed, as shown in the numerical results of Pillai and Yoshie (2012). With regard to the relationship between the length of a scalar source in the upwind fetch and $C_{\mathrm{E\,wet}}$, street surfaces surrounded by block arrays with high $\lambda_{\mathrm{p\text{-}block}}$ condition are less affected compared to sparse block arrays and smooth surfaces. The estimated scalar transfer coefficients defined by flux per lot-area $C_{\mathrm{E\,lot}}$ of both wet streets of block arrays and wet smooth surfaces with dry patches clearly demonstrate the oasis effect due to the heterogeneous scalar source allocation. The $C_{\mathrm{E\,lot}}$ values of a wet smooth surface with dry area ratio of 31 % still exceed those of a fully wet smooth surface in spite of the smaller scalar source area.

The experimental results were also analyzed using the variable $B'^{-1}(= C_{\mathrm{E}}^{*-1} - C_{\mathrm{m}}^{*-0.5})$, which is approximately equivalent to $\kappa^{-1} \ln(z_{\mathrm{o}}/z_{\mathrm{os}})$. The data for two contrasting measurement conditions, dry cube arrays located on a wet street surface, and wet smooth surfaces with dry square patches, clearly show that $z_{\mathrm{os}}$ for smooth surfaces increases strongly because of the heterogeneous scalar source allocation. In addition, the aerodynamic effect of the present block arrays results in a much larger $z_{\mathrm{o}}$ compared to $z_{\mathrm{os}}$, while $B'^{-1}$ for block arrays varies with topography in spite of similar $Re^*$ conditions.

**Acknowledgments** We are grateful to Dr. Ken-Ichi Narita for his valuable suggestions and for allowing us to use the salinometer of his laboratory for this experiment. This project was partly funded by the Ministry of Education, Science, and Culture of Japan (Grant-in-Aid for Scientific Research 25289196). We would also like to thank the referees for careful reading of the manuscript and helpful comments.

## References

Anderson W (2013) Passive scalar roughness lengths for atmospheric boundary layer flow over complex, fractal topographies. Environ Fluid Mech 13:479–501

Barlow JF, Belcher SE (2002) A wind tunnel model for quantifying fluxes in the urban boundary layer. Bound Layer Meteorol 104:131–150

Barlow JF, Harman IN, Belcher SE (2004) Scalar fluxes from urban street canyons. Part 1: Laboratory simulation. Bound Layer Meteorol 113:369–385

Blocken B, Defraeye T, Derome D, Carmeliet J (2009) High-resolution CFD simulations for forced convective heat transfer coefficients at the facade of a low-rise building. Build Environ 44:2396–2412

Brutsaert W (1982) Evaporation into the atmosphere. Kluwer Academic Publishers, Dordrecht

Brutsaert W (1975) A theory for local evaporation (or heat transfer) from rough and smooth surfaces at ground level. Water Resour Res 11:543–550

Chamberlain AC (1968) Transport of gases to and from surfaces with bluff and wave-like roughness elements. Q J R Meteorol Soc 94:318–332
Cheng H, Castro IP (2002) Near wall flow over urban-like roughness. Bound Layer Meteorol 104:229–259
Defraeye T, Blocke B, Carmeliet J (2010) CFD analysis of convective heat transfer at the surfaces of a cube immersed in a turbulent boundary layer. Int J Heat Mass Transf 53:297–308
Defraeye T, Blocken B, Carmeliet J (2011) Convective heat transfer coefficients for exterior building surfaces: existing correlations and CFD modelling. Energy Convers Manag 52:512–522
Garratt JR (1994) The atmospheric boundary layer. Cambridge University Press, UK, 316 pp
Garratt JR, Hicks BB (1973) Momentum heat and water vapour transfer to and from natural and artificial surfaces. Q J R Meteorol Soc 99:680–687
Grimmond CSB, Oke TR (1999) Aerodynamic properties of urban areas derived from analysis of surface form. J Appl Meteorol 38:1262–1292
Hagishima A, Tanimoto J, Narita K (2005) Intercomparisons of experimental convective heat transfer coefficients and mass transfer coefficients of urban surfaces. Bound Layer Meteorol 117:551–576
Hagishima A, Tanimoto J, Nagayama K, Meno S (2009) Aerodynamic parameters of regular arrays of rectangular blocks with various geometries. Bound Layer Meteorol 132:315–337
Hagishima A, Narita K, Tanimoto J (2007) Field experiment on transpiration from isolated urban plants. Hydrol Process 21:1217–1222
Ikegaya N, Hagishima A, Tanimoto J, Tanaka Y, Narita K, Zaki SA (2012) Geometric dependence of the scalar transfer efficiency over rough surface. Bound Layer Meteorol 143:357–377
Incropera F, DeWitt D (2002) Fundamentals of heat and mass transfer, 5th edn. Wiley, New York, 455 pp
Kanda M, Moriizumi T (2009) Momentum and heat transfer over urban-like surfaces. Bound Layer Meteorol 131:385–401
Kanda M, Kanega M, Kawai T, Moriwaki R, Sugawara H (2007) Roughness lengths for momentum and heat derived from outdoor urban scale models. J Appl Meteorol Climatol 46:1067–1079
Kanda M, Inagaki A, Miyamoto T, Gryschka M, Raasch S (2013) A new aerodynamic parametrization for real urban surfaces. Bound Layer Meteorol 148:357–377
Macdonald RW, Griffiths RF, Hall DJ (1998) An improved method for estimation of surface roughness of obstacle arrays. Atmos Environ 32:1857–1864
Millward-Hopkins JT, Tomlin AS, Ma L, Ingham D, Pourkashanian M (2011) Estimating aerodynamic parameters of urban-like surfaces with heterogeneous building heights. Bound Layer Meteorol 141:443–465
Moriwaki R, Kanda M (2004) Seasonal and diurnal fluxes of radiation, heat, water vapor and CO2 over a suburban area. J Appl Meteorol 43:1700–1710
Narita K (2007) Experimental study of the transfer velocity for urban surfaces with a water evaporation method. Bound Layer Meteorol 122:293–320
Owen PR, Thomson WR (1963) Heat transfer across rough surfaces. J Fluid Mech 15:321–334
Pascheke F, Barlow JF, Robins A (2008) Wind-tunnel modelling of dispersion from a scalar area source in urban-like roughness. Bound Layer Meteorol 126:103–124
Pillai SS, Yoshie R (2012) Experimental and numerical studies on convective heat transfer from various urban canopy configurations. J Wind Eng Ind Aerodyn 104–106(4):447–454
Zaki SA, Hagishima A, Tanimoto J, Ikegaya N (2011) Aerodynamic parameters of urban building arrays with random geometries. Bound Layer Meteorol 138:99–120